ASEAN Journal of Chemical Engineering 2025, Vol. 25, No. 2, 310–323

Production of Hydrogen with Electrolysis-Photovoltaic from Seawater Using Ni-Mo Electrodes Deposited at Cu (Ni-Mo/Cu)

Shafa Nabilah [*,1]
Hanun Salbila Marhaenetry [1]
Mepa Maftuha Prizantika [2]
Lalak Tarbiyatun Nasyin Maleiva [*,1]
[1] *Chemical Engineering Department, Faculty of Engineering, Tanjungpura University, Pontianak 78124, Indonesia*
[2] *Electrical Engineering Department, Faculty of Engineering, Tanjungpura University, Pontianak, 78124, Indonesia*
*e-mail: heloshafana@gmail.com (S.N.); lalaktnm@teknik.untan.ac.id (L.T.N.M.)

Submitted 19 November 2024 *Revised* 30 July 2025 *Accepted* 8 August 2025

Abstract. The energy crisis and environmental impacts of fossil fuels encourage the development of environmentally friendly alternative energy sources. Hydrogen is a promising candidate as a future energy carrier. This research aims to optimize hydrogen production through seawater electrolysis using Ni–Mo/Cu electrodes with a photovoltaic energy source. Ni–Mo/Cu electrodes were prepared via electrodeposition at a varied durations of 2, 4, and 6 minutes. Electrode characterization was conducted using X-Ray Diffraction (XRD) and Scanning Electron Microscope-Energy Dispersive X-Ray (SEM–EDX). Photovoltaic systems were designed using fuzzy logic to optimize solar energy absorption. The electrolysis process was carried out at voltages of 10–30 V. The results showed that a 4-minute electrodeposition produced the most significant Ni–Mo layer. The highest hydrogen production rate of 0.7417 cm^3/s was obtained at 25 V using a Ni–Mo/Cu electrode. These findings demonstrate the feasibility of producing hydrogen from seawater using renewable energy sources under the studied conditions.

Keywords: Electrodeposition, Electrolysis, Hydrogen, Ni-Mo/Cu Electrodes, Photovoltaic

INTRODUCTION

Almost all human activities are relatively dependent on the availability of energy, which is why energy is a critical component of human survival (House J. E. & House K. A., 2016). Indonesia is not the only country affected by the energy crisis; it is a global issue. The energy transition is also supported by numerous factors, such as the impact of carbon emissions generated by fossil energy and energy security (Cho *et al*., 2022; Siddiqui *et al*., 2019; Finke *et al*., 2021). The International Energy Agency (IEA) has devised a net-zero emission energy plan that aims to increase the use of hydrogen as a basic material or energy carrier to 24% of energy demand by 2050 (Srour *et al*., 2024). This matter motivates numerous stakeholders to pursue environmentally favorable energy sources, including hydrogen gas. Hydrogen is anticipated to be a future alternative fuel that is both environmentally favorable and efficient (Sangian *et al*., 2023). The energy

DOI: 10.22146/ajche.17741

supply it generates is both pure and emission-free, as it only produces water vapor as a by-product during the production process. To resolve the global energy crisis, hydrogen has emerged as one of the most critical alternative energy sources in recent years (Avci & Toklu, 2022).

Natural gas, petroleum, and coal refining are the primary methods of hydrogen production, accounting for 95% of the total. In the interim, electrolysis accounts for 5% of the global hydrogen production process (Gielen *et al*., 2019; Chi & Yu, 2018). Water electrolysis has garnered attention due to its environmental friendliness, its utilization of water as an infinite resource, and its low production cost (Zhang & Ashraf, 2020). This method offers the benefit of a straightforward water molecular decomposition process, while also being capable of producing hydrogen gas with a high level of purity. Indonesia is a tropical country, and the city of Pontianak, which straddles the phase line, presents a significant opportunity to produce hydrogen gas using a photovoltaic cell energy source. Rahwanda *et al*., (2022) conducted research that supports this assertion, indicating that the monthly average of solar radiation intensity in Pontianak City was 3.31-5.25 kWh/m^2 over 10 years from 2009-2018. Nevertheless, the production of electricity may be unstable due to fluctuations in the intensity of daily solar radiation. Consequently, this instability can be resolved by incorporating a variety of devices, including the BH175 sensor and the LDR sensor as light intensity sensors, the Arduino UNO, the NodeMCU, and the use of Fuzzy logic to move the servo to align the photovoltaic cell with the sunlight (Arachman *et al., 2023*). In addition to reducing the cost of hydrogen production through photovoltaic electrolysis, it is imperative to enhance production efficiency. For instance, the inclusion of ions as electrolytes can increase conductivity. Nevertheless, the production of hydrogen by large-scale electrolysis necessitates a substantial amount of water and salt. Consequently, alternative sources, such as natural electrolyte solutions for electrolysis, generate hydrogen, including seawater.

Seawater is composed of 96.5% purified water and 3.5% other materials, including saline elements, dissolved gases, organic matter, and insoluble particles (Prastuti, 2017). Due to its abundance and wide availability, seawater is a promising electrolyte for hydrogen production. Its use also supports the development of hydrogen production technologies based on renewable energy sources. Indonesia, being located along the equator and having extensive coastal areas, holds significant potential in utilizing seawater for energy applications. Given that two-thirds of its geographical area is made up of oceans, Indonesia is acknowledged as the largest maritime nation in the world. 71% of the Earth's surface is covered by water, and 96.5% of the planet's water supply comes from seawater (Kim & Lee, 2022). Therefore, the potential for the widespread application of hydrogen production through the electrolysis of seawater to expedite the transition from fossil fuels is significant.

The selection of seawater as an electrolyte is based on its conductivity and availability, as well as its alignment with clean energy goals. The optimal electrode should exhibit high catalytic activity, excellent conductivity, and resistance to seawater corrosion. Therefore, to enhance conductivity and corrosion resistance, several electrodes were investigated such as graphene (Wehrhold *et al.,* 2022), rhodium (Devendra *et*

al., 2022), Pt-Ni (Carro *et al.* 2023), Ni-Mo (Liu *et al.* 2022; Zhang and Ashraf, 2020; Aguilar *et al.* 2024), Ni-Co (Hüner *et al.,* 2023; Yang, 2022), Ni-Fe (Wang *et al.* 2023), Ni-SnO_2 (Xing *et al.,* 2022), PtNb-Nb_2O_5 (Nie *et al.,* 2022), and composites based on Nb superconductor (Franceschini *et al.,* 2022; Prysyazhnyuk *et al.,* 2018; Dubrovskiy *et al.,* 2018). However, nickel is regarded as a great option among the transition metals due to its lower free energy required to absorb hydrogen. Moreover, Ni-Mo alloys have been discovered as one of the best binary alloys for the water electrolysis process (Zhang & Ashraf, 2020). On the other hand, Cu lies in the volcano plot just below Pt and MoS_2 due to its favorable exchange current density and DGH in terms of HER. Still, its greatest barrier is its susceptibility to corrosion (Yowanda & Lestari, 2021). Therefore, to enhance conductivity and corrosion resistance, Ni–Mo electrodes were sparsely deposited onto copper surfaces (Ni–Mo/Cu) using electrodeposition techniques. The resulting nanostructured coating can increase the electrochemically active surface area, thus enhancing hydrogen evolution reaction (HER) performance (Zhang & Ashraf, 2020; Yang et al., 2019; Nairan et al., 2020).

The objective of this research is to investigate the effect of electrodeposition duration on the characteristics of Ni–Mo electrodes on Cu substrates and to evaluate their performance in seawater electrolysis powered by solar photovoltaic systems. The study also aims to examine the effect of applied electrical voltage on the hydrogen generation rate using the Ni–Mo/Cu electrode. It is expected that the findings can support advancements in the production of hydrogen from seawater with both efficient and cost-effective outcomes. This work also highlights the potential of utilizing Indonesia's abundant seawater and renewable solar energy in contributing to national energy sustainability.

MATERIALS AND METHODS

The following materials were employed in this research: acetone, distilled water, Ag/AgCl electrodes, aluminium foil, ethylenediamine (EDA), HCl 20%, 0.5 M H_3BO_3, 1.0 M $NiCl_2.6H_2O$, and 0.1 M Na_2MoO_4, copper rod (Cu), and graphite rod.

Stage of Solution Preparation and Electrocatalyst Manufacturing

The Ni-Mo layer was deposited on the copper electrode (Cu) surface using an electrodeposition method that commence with the cutting of a Cu rod with a diameter of 10 mm and a length of 4 centimeters, followed by embossing with grit 2000. The electrode was produced by depositing a Ni-Mo layer on the surface of a copper rod (Cu) that had been previously prepared. The degreasing process was conducted in acetone for 20 minutes. The sample was subsequently immersed in a 20% HCl solution for 20 seconds to activate it. The sample was subsequently rinsed with aquadest. Coating was performed on a standard three-cell electrode, with Ag/AgCl serving as the reference electrode, which was situated near the working electrode. Samples were prepared as working electrodes, while graphite bars were employed as the system electrode. The electrodeposition method was employed to deposit Ni-Mo layers at 10 volts (potentiostatic). The immersion coating's composition was as follows: 0.5 M H_3BO_3, 1.0 M $NiCl_2.6H_2O$, and 0.1 M Na_2MoO_4. EDA was employed to produce the crystal pattern at a rate of up to 200 g/L. The coating was applied at a current density of 500 mA cm^{-2} (Zhang *et al.,* 2020) for 2, 4, and 6 minutes, and the

coating was subsequently desiccated.

Characterization of the Electrode

To analyze the surface morphology of the porous size distribution of the electrode and to observe the homogeneity of the deposited Ni-Mo layer, the deposited Ni-Mo layer was characterized using SEM-EDX. To distinguish the crystalline phase of the Ni-Mo/Cu layer and ascertain the phase composition of the metal oxide in the constituting layer of the electrode, XRD tests were also implemented.

Characterization of the Properties of Seawater

The salinity, pH, and conductivity of seawater were initially assessed before electrolysis after they were collected from the coast of the Bengkayang district, West Kalimantan Province. The pH measurement was conducted using a pH meter that was calibrated to the standard pH range of 7.5-8.4.

Photovoltaic Radiation Stage

This research employed an Arduino UNO microcontroller with the Fuzzy Sugeno logic decision-making method. The input values of the TEMT6000 east and TEMT600 west sensors were processed using the trimf membership function, which has a range of 0-1050. The output was servo values with a range of 0-10, which were used as a determinant of the motion of the servo motor MG996R as a photovoltaic propeller. The BH1750 was employed as a solar intensity meter to ascertain the surrounding weather. The INA219 sensor was employed to obtain current and voltage values. The MCU Node, a microcontroller, processes data on the intensity of light, voltage, current, and power from the photovoltaic cell, then sends it to a Google Spreadsheet and Firebase database for monitoring. The data was then displayed in real time by a monitoring application created using Android Studio software. The survey was conducted from 8:00 AM to 4:00 PM.

Electrolysis of Seawater

The electrolysis device was assembled after the electrode preparation. The system included a potentiostat operating in galvanostatic mode to apply a controlled current. Electrolysis was conducted using optimally deposited Ni–Mo/Cu electrodes and a graphite bar as the counter electrode. The temperature was maintained at room temperature. During electrolysis, the hydrogen gas produced was captured in a water displacement setup, and the gas volume was measured using a manometer over time intervals to calculate the hydrogen evolution rate. The volume of hydrogen gas is measured by calculating the dimensions (cm^3) of the space in the glass reactor that occurs due to the formation of hydrogen gas and pushing water to the side of the manometer.

The level of homogeneity and uniformity of the Ni-Mo/Cu electrode layer resulting from the deposition will be determined by analyzing the Ni and Mo atomic composition of the layer obtained from the SEM-EDX characterization results. The crystal phase and orientation formed are determined by analyzing the diffraction patterns and peak intensity results of the XRD characterization on the layer. Additionally, the hydrogen volume data produced during electrolysis was analyzed and curved to determine the impact of voltage on the hydrogen content. The impact of voltage was assessed by altering it at 10-30 Volts in 5 Volt increments, maintaining a constant voltage

(potentiostatic) throughout the electrolysis process. The addition of EDA and an extended electrodeposition time induces the formation of nanostructures on the Ni-Mo/Cu electro-catalyst surface as a result of the growth stimulus of vertical electrochemistry. The optimal electrodeposition time can be determined by comparing the peak intensity of the diffractogram to the XRD analysis result. The volume of hydrogen produced from voltage fluctuations during the marine water electrolysis process can be used to determine the optimal electrical voltage. The surface morphology of the porous size distribution of the electrode and the homogeneity of the deposited Ni-Mo layers were analysed by utilizing SEM to characterize the deposited Ni-Mo layers. The phase composition of the metal oxide component of the electrode layer is determined through XRD tests.

RESULTS AND DISCUSSION

Characteristics of Seawater

The seawater utilized is sourced from Gratis Beach in Bengkayang. The seawater has a salinity of 31.54 ppt, a pH of 7.5, and a temperature of 31.8 °C. It contains 39 grams/mL of ions (Yowanda & Lestari, 2021). The high conductivity of seawater is a result of its salinity and salt content, which can aid in the production of additional hydrogen gas during the electrolysis process.

Production of Ni-Mo/Cu Electrodes

The Ni–Mo layer was electrodeposited onto the surface of copper bars (Cu) during the electrode manufacturing procedure in this investigation. A standard three-electrode cell was employed, with Ag/AgCl serving as the reference electrode. It was placed near the working electrode to ensure accurate control of the applied potential during the coating process. This setup allowed for stable and consistent deposition conditions. Figure 1 illustrates the outcome of the electrodeposition.

(a) (b) (c)

Fig. 1: Results of electrodeposition (a) 2 minutes; (b) 4 minutes; and (c) 6 minutes

A Ni-Mo layer, which is a green crystalline fragment, has been deposited on the copper surface following this procedure, as evidenced by XRD and SEM characterization.

XRD Characterization Results

The objective of this analysis is to ascertain the influence of time variations on the coating. The following image illustrates the diffractogram of Ni-Mo/Cu electrodeposition results for 2, 4, and 6 minute variations:

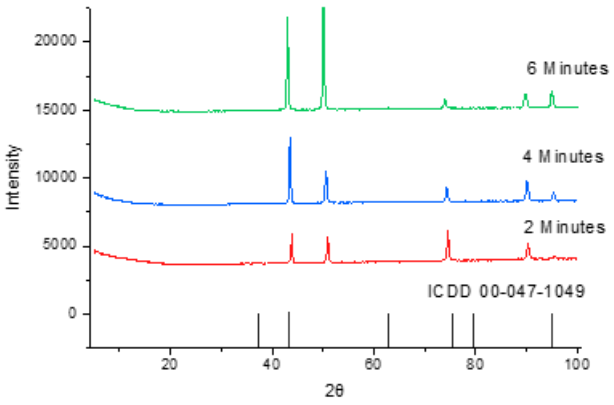

Fig. 2: The diffractogram of the Ni-Mo/Cu coating as a function of time

The XRD analysis revealed the presence of dominant diffraction peaks at angles of 2θ

43.8489°, 50.8824°, 74.5082°, 90.1661°, and 95.5289°, after a 2-minute variation in electrodeposition time. The principal component is copper (Cu), as indicated by this diffraction pattern. Additionally, there is a potential for the detection of a copper-nickel alloy phase (Ni-Cu) with a score of 27. At peak points 43.8489° (100%), the relative intensity was the highest, followed by peaks at 74.5082° (96.27%) and 50.8824° (83.35%).

The XRD analysis of a sample with electrodeposition time variation for 4 minutes revealed a diffraction pattern, with the primary peaks located at angles 2θ 43.5444°, 50.5515°, 74.2559°, 90.0059°, and 95.2461°. The apex peak was detected at 43.5444° with a relatively high intensity of 100%. The presence of copper (Cu) as the primary component was indicated by phase identification, which has a matching point of 77. Additionally, there were indications of the presence of nickel oxide (NiO) with a matching score of 11, albeit in relatively small quantities. This diffraction pattern is in accordance with the predominant copper crystal structure, with the potential for a minor quantity of nitric oxide to exist as a secondary phase.

A diffraction pattern with the primary peaks at 2θ angles of 42.9468°, 50.0347°, 73.9448°, 89.7428°, and 94.8490° is observed in the XRD analysis of a sample with a variation in the electrodeposition duration for 6 minutes. The relative intensity of the highest peak is 100% at 50.0347°, and it is followed by a peak at 42.968° with a relative strength of 76.35%. A score of 50 matches indicates the presence of copper (Cu) as the primary component, as indicated by the phase identification. This diffraction pattern suggests that the sample was primarily composed of copper crystal structures, with the potential for a small quantity of nickel oxide to exist as a secondary phase.

The analysis of copper coating diffractogram patterns (Ni-Mo/Cu) was conducted within a 2θ-10° angle range. With successive intensities of 67.9, 100, 43, 7, 14.3, 10.4%, and 3.7%, the highest peaks on the data reference code 03-065-5745 are 37.23°, 43.29°, 62.88°, 75.42°, 79.41°, and 95.07°. The XRD result in Figure 2 indicates that the coating result is the result of the appearance of peaks that are near the reference data code 03-065-5745 on electrodepositions with a time variation of 4 minutes. By the ICDD standard 00-047-1049, the identification process revealed peaks at 43.54° and 95.25° with a high intensity of 100%.

Results of the SEM Analysis

The structural relationships between the variables associated with the Ni-Mo/Cu compounds were investigated through the SEM analysis. Analysis of the copper (Cu) surface stratified with Ni-Mo was conducted at a magnification of 5,000x, with the sample examined three times. The nanostar structure that was anticipated was evident in the SEM results of the three samples. Based on the research journal Zhang and Ashraf (Zhang & Ashraf, 2020), the nanostar structure on the Cu surface can be observed using SEM at a magnification of 5,000x. However, the nanostar structure did not appear in this study after the SEM analysis was conducted at the same magnification.

In Figure 3(a), the surface of the sample treated for 2 minutes shows an asymmetrical texture, characterized by scattered bright particles on a darker background. This indicates non-uniform topographic composition and suggests areas of high particle concentration. The bright particles range in diameter from approximately 0.5 to 1 μm. Some larger clusters can also be

observed. The surface contains microfractures forming irregular patterns, suggesting a rough and discontinuous structure.

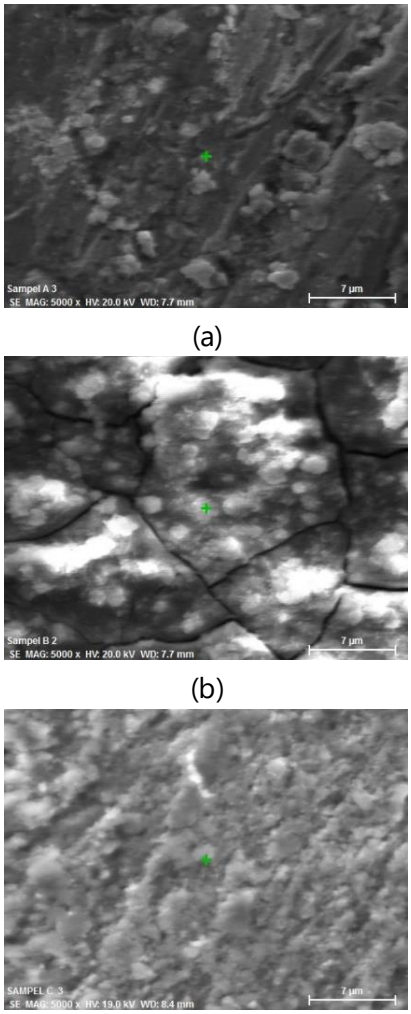

Fig. 3: The Ni-Mo/Cu surface morphology from varied electrodeposition time: (a) 2 minutes; (b) 4 minutes; and (c) 6 minutes

In Figure 3(b)**,** the surface morphology of the samples with a 4-minute coating treatment was highly complex and heterogeneous, as evidenced by the SEM analysis results. Particle agglomerations of varying sizes, ranging from fine fragments to larger clusters, as well as stratified structures with rugged and irregular texture, dominate surfaces. Certain regions appear to be more illuminated, suggesting variations in material composition or height. Fine fissures were present in certain regions of the surface. This morphology suggests a very high surface area.

In Figure 3(c), the SEM analysis of a sample that experienced a 6-minute coating treatment revealed that the material's surface structure is highly porous and textured on a micron scale. The material was composed of numerous tiny, irregularly shaped particles or aggregates that collectively form intricate and interconnected tissues. The surface exhibits a substantial degree of rigidity and topographic variation, evidenced by the presence of visible fissures or spaces that may suggest the fragility of the sample preparation results.

Result of the EDX Analysis

Based on the results of EDX analysis of the copper (Cu) surface coated with nickel molybdenum (Ni-Mo), it is indicates that the electrodeposition with 2 minutes shows the surface composition with the main content of Cu (97.95% by weight), as well as Ni (1.77% by weight) and Mo (0.28% by weight). This composition indicates that the sample surface is dominated by a layer of copper, with a small content of nickel and molybdenum. The percentage of Cu atoms (97.90%) is much higher than that of Ni (1.92%) and Mo (0.18%), indicating that the layer of Cu has covered almost the entire surface. These results indicate that the process of Ni-Mo coating on the copper surface has been successfully carried out, and Cu coating dominates the surface with relatively small Ni and Mo contents.

Electrodeposition time of 4 minutes shows the surface composition with the main content of Mo (97.99% by weight), as well as Ni (1.20% by weight) and Cu (0.80% heavy).

This composition indicates that the sample surface is dominated by a molybdenum layer, with small amounts of nickel and copper. Atomic percentage Mo (96.86%) is much higher than Ni (1.94%) and Cu (1.20%), indicating that the Mo layer had covered most of the surface. This result shows that the Mo coating process on the surface has been successfully carried out, and the Mo layer dominates the surface, but there is still a small amount of Ni and Cu that is exposed.

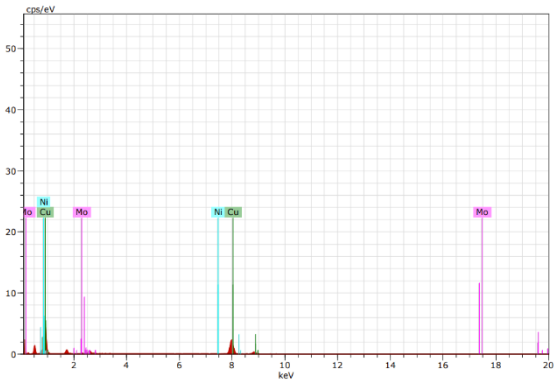

Fig. 4: EDX Spectrum of Ni-Mo/Cu coating at time variation of 2 minutes

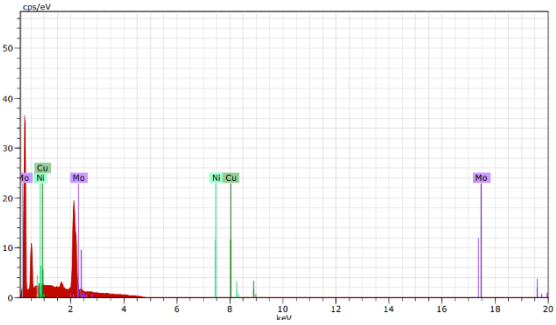

Fig. 5: EDX spectrum of Ni-Mo/Cu coating at time variation of 4 minutes

Electrodeposition with a time of 6 minutes shows the surface composition with the main content of Cu (72.42% by weight) and Ni (13.80% by weight), as well as Mo (13.77% by weight). This composition indicates that the copper surface has been coated with a mixture of nickel and molybdenum. The percentage of Cu atoms (75.06%) is higher than that of Ni (15.49%) and Mo (9.45%), indicating that the Ni-Mo layer does not cover the entire copper surface. These results suggest that the Ni-Mo coating process on the Cu surface has been successfully carried out. However, the coating is not evenly distributed, with still areas of exposed copper.

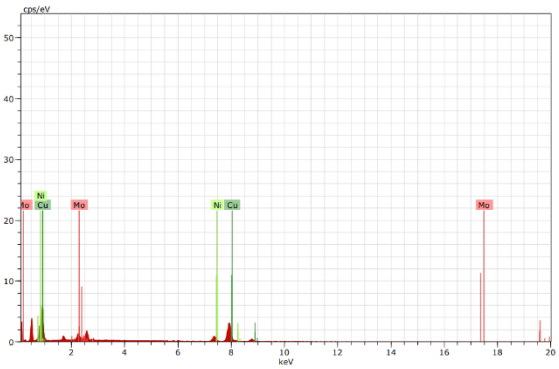

Fig. 6: EDX spectrum of Ni-Mo/Cu coating at time variation of 6 minutes

Table 1. Elemental composition of samples based on EDX analysis

Sample	EDX Spectrum	Element	% Wt
2-minute	Figure 4	Ni	1.77
		Mo	0.28
		Cu	97.95
4-minute	Figure 5	Ni	1.20
		Mo	97.99
		Cu	0.80
6-minute	Figure 6	Ni	13.80
		Mo	13.77
		Cu	72.42

Overall, the EDX analysis results confirm that the copper surface was successfully coated with a Ni–Mo layer, although the coating quality varied depending on the deposition duration. Table 1 shows the Cu electrode subjected to a 4-minute electrodeposition showed the highest Mo content, indicating a more effective coating and dominance of the active catalytic metal. In contrast, electrodes with 2-minute and 6-minute deposition times exhibited incomplet

e coverage, with Cu signals still dominant, implying that insufficient or excessive deposition time may hinder optimal metal deposition.

Based on a previous study, an effective Ni–Mo catalyst layer should exhibit a uniform and Mo-rich surface for optimal hydrogen evolution reaction (HER) performance (Zhang & Ashraf, 2020). The 4-minute sample in this study appears to meet this criterion, suggesting it possesses adequate catalytic properties for the intended application. Therefore, this sample is considered suitable for further electrochemical performance testing. However, further validation through electrochemical characterization is recommended to confirm catalytic efficiency and stability.

Photovoltaic Assembly

The photovoltaic assembly preparations commenced with the assembly of lithium-ion batteries. Twelve batteries were constructed in a succession of four series and three parallel configurations. Batteries are equipped with battery management systems (BMS) to ensure their security. The voltage that enters a 50-watt photovoltaic cell was determined by connecting it to a wattmeter. The voltage is then transferred to the SCC, which functions as a 20-amp photovoltaic controller. The photovoltaic controller is then connected to the battery. The photovoltaics affixed on the framework can be moved to the left and right sides by using the TEMT6000 sensor on the right and left sides. This sensor will transmit values to the servo, which will adjust the photovoltaic's direction toward the sun when high light intensity values are detected. Both are constructed using the Fuzzy Sugeno logic system to determine the positions of the photovoltaic panels about the sun's direction, thereby maximizing solar energy. If the right sensor is 75.5 and the left sensor is 38.3, the servo output will be 123, which will result in the right, as the sunlight is more intense on the right. This is based on a single rule. The subsequent table displays the measurement data results.

The amplitude of the voltage generated by the solar panel is influenced by the difference in light intensity caused by the level of luminosity and the cloud cover. Therefore, the panel is oriented by the sun's direction to capture the maximum amount of sunlight. The sensor receives the most significant light in strong sun conditions within the temperature range of 28 °C to 33 °C. The intensity of the sun's rays fluctuates due to the amount of sunlight that is obscured by clouds during the output voltage testing of solar panels. The data obtained shows that the maximum values for the intensity of light, voltage, current, and power were observed at 11:00 PM during the hourly measurement of 08:00 – 04:00 PM.

Table 2. Intensity of light, voltage, current, and power per hour

Time	Intensity of Light (Lux)	Voltage (Volt)	Current (A)	Power (Watt)
08:00	65,200	17.05	0.32	5.45
09:00	75,200	18.20	0.42	7.64
10:00	103,100	19.86	0.49	9.73
11:00	107,300	19.89	0.51	10.14
12:00	95,250	19.78	0.48	9.49
13:00	89,000	19.60	0.46	9.01
14:00	78,400	19.34	0.44	8.50
15:00	68,300	17.08	0.33	5.63
16:00	63,100	16.80	0.23	3.86

Table 2 shows the data subsequently serves as a baseline to ascertain the energy storage

capacity and to strategize for more stable electrolysis system operations, hence mitigating fluctuations in the electrical energy supply during the electrolysis process.

Electrolysis of Seawater

Overall, the EDX analysis indicates that the copper surface was successfully coated with a mixture of nickel and molybdenum (Ni–Mo), although the degree of coating varies with deposition time. The electrode deposited for 4 minutes exhibits the highest Mo content and the most uniform surface coverage, suggesting a more effective and stable catalytic layer. In contrast, electrodes with 2-minute and 6-minute deposition durations still show dominant copper signals, indicating either insufficient deposition (2 minutes) or possible overgrowth and delamination (6 minutes), which may reduce coating integrity.

According to previous literature, a Mo-rich Ni–Mo layer is desirable for optimal catalytic activity in hydrogen evolution reactions (Zhang & Ashraf, 2020). The 4-minute sample in this study aligns with those findings, indicating its potential suitability for further electrochemical evaluation. These results suggest that the 4-minute deposition condition provides a balanced composition and morphology, likely sufficient to support the next stage of performance testing.

Voltage is one of the variables that can influence the volume of hydrogen gas generated. It is evident from Figure 7(a) that the production of hydrogen gas increases as the voltage increases. The first Faraday's law is directly analogous to this, in which the quantity of substance generated on an electrode is precisely proportionate to the electrical charge (Herlambang *et al.*, 2020), where electrical charge is the number of current during a certain period (current x time), and current has a direct proportionality to voltage. At a constant resistance, as current rises, voltage rises linearly, thus it eventually increases the gas generated.

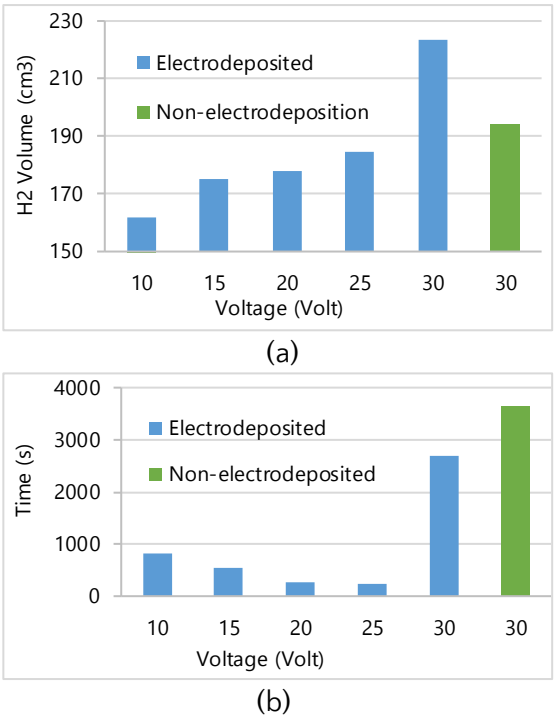

Fig. 7: The impact of voltage on (a) the volume of hydrogen; and (b) the duration of hydrogen production

Both the voltage and the volume influence the duration of the electrolysis procedure. In this study, the duration of the electrolysis process was recorded until the water level in the reactor peaked, driven by the propulsion of hydrogen gas generated on the cathode side. This measurement facilitates a comprehensive comparison of the production time and efficiency achieved. According to Figure 7(b), the electrolysis process time was reduced by up to 249 seconds at a voltage of 25 V as the voltage increased. Nevertheless, the energy consumption was greater at a 30 V voltage, which results in a prolonged production time of 2690 seconds, rendering the process ineffective in the production of hydrogen gas

with a higher volume. Nonetheless, the extended production time observed at 30 V might indicate that the applied potential has surpassed the effective range for hydrogen evolution, leading to a diminished driving force for the reaction. As a result, the process exhibits reduced efficiency even with the increased voltage input. This aligns with the findings of Nascimento *et al.* (2023), who confirmed that energy consumption rises with an increase in voltage. The rise in this phenomenon could originate from the electrolysis system's inefficiencies, including significant overpotential, which leads to a reduction in efficiency at elevated voltages, despite an increase in gas production. This is also the case when an electrolysis process was conducted at the same voltage as an electrode without a deposition. This illustrates the substantial influence of the electrodeposition process, as it can enhance electrocatalytic activity, enabling the Ni-Mo/Cu electrodes to complete electrolysis processes in a shorter timeframe than undeposited copper electrodes. The substantial impact of this electrodeposition ultimately influences the flow rate of the hydrogen gas production.

In addition, voltage not only affects the flow rate and volume of hydrogen generated but also significantly influences the length of the electrolysis process. Figure 7(b) indicates that while increased voltage generally enhances hydrogen generation, excessively high levels, like 30 V, can lead to reduced efficiency. This is attributed to factors such as overpotential, electrode degradation, and internal resistance, which ultimately result in extended processing times. This suggests that the ideal voltage is not necessarily the maximum, but rather the level that maintains a balance among speed, efficiency, and system stability.

As illustrated in Figure 8(a), the hydrogen gas flow rate was measured during electrolysis using a water displacement method, and the values were recorded in units of cm^3/s. The hydrogen gas flow rate has increased the most at a voltage of 25 V, with a value of 0.7417 cm^3/s. A high flow rate signifies quick gas production; however, if the duration of electrolysis is brief, the overall gas volume remains small. With a voltage variation of 25 V, the electrolysis process concludes more rapidly, even with a high gas flow rate, leading to a reduced total gas volume. The flow rate is significantly different, with hydrogen produced at a non-deposition electrode at the highest electrolysis voltage (30 V) being four times smaller than that produced at a 10 V voltage with Ni-Mo-deposited Cu electrodes.

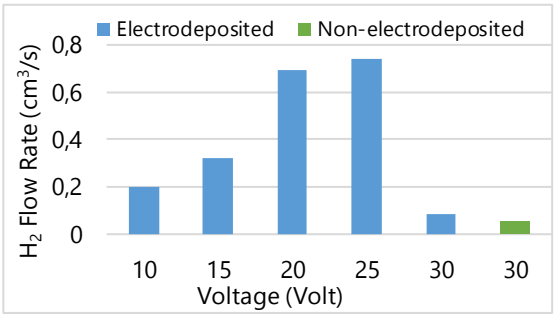

(a)

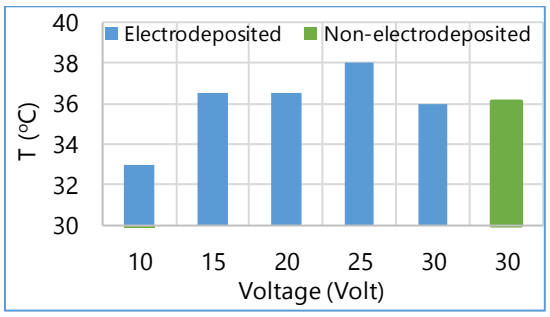

(b)

Fig. 8: The impact of voltage on (a) the hydrogen flow rate; (b) and temperature

This demonstrates that the active surface area of the Cu electrode is greater than that of the undeposited Cu electrodes due to the

existence of the Ni-Mo layer on the Cu electrode surface. This is consistent with the findings regarding the voltage's impact on the volume of hydrogen gas and the duration of the electrolysis process. Consequently, the optimal voltage for this electrolysis procedure is 25 V. This conclusion is corroborated by the correlation between the resulting electrolyte temperature after electrolysis and the applied voltage, as illustrated in Figure 8(b).

The temperature of the electrolysis process generally increases as the voltage increases, as illustrated in Figure 8(b). However, at 30 V, the temperature drops due to the absence of significant electrolysis activity, especially at the non-electrodeposited electrode, which results in lower heat generation. Consequently, the electrolysis device will become increasingly heated as the voltage increases. This temperature rise will increase the electron's kinetic energy, which will accelerate the reduction-oxidation reaction.

CONCLUSIONS

Ni-Mo/Cu electrodes are employed in marine water photovoltaic electrolysis methods, which demonstrate promising potential as environmentally benign and sustainable alternatives to hydrogen production, particularly in coastal or island regions. The research results indicate that Ni-Mo electrodeposition on a copper surface (Cu) was effectively conducted with an optimal deposition time of 4 minutes, resulting in the most optimal Ni-Mo layer as determined by XRD and SEM analysis. In comparison to Cu electrodes without deposition, the Ni-Mo/Cu electrodes showed improved performance compared to bare Cu electrodes in the marine water electrolysis process, as evidenced by a higher hydrogen flow rate and shorter electrolysis duration, as well as their ability to generate a greater volume of hydrogen gas and achieve reduced electrolyte time. The maximum hydrogen flow rate of 0.74 mL/s was achieved when the optimal voltage for hydrogen production through marine photovoltaic-electrolysis-water using Ni-Mo/Cu electrodes was 25 V. The optimization of power generation for electrolysis processes can be achieved through the use of photovoltaic systems with solar tracking technology combined with fuzzy logic.

ACKNOWLEDGEMENT

The research can be conducted effectively with the assistance of a variety of parties. The researchers are extremely grateful to the Directorate General of Higher Education, Research, and Technology (DITJEN DIKTIRISTEK) of Indonesia through the Directorate of Learning and Study (BELMAWA), Tanjungpura University, and the Chemical Engineering Laboratory of Tanjungpura University for their assistance and support in conducting this research.

REFERENCES

Arachman, F. D., Antony, F., and Rachmansyah, 2023. "Sistem kendali penggerak sel fotovoltaik menggunakan logika fuzzy dengan sensor lux berbasis internet of things." *J. Intell. Netw. IoT* Global, *1(1)*, 33-38.

Avci, A. C. dan Toklu, E., 2022. "A new analysis of two phase flow on hydrogen production from water electrolysis." *Int. J. Hydrog. Energy, 47(11)*, 6986-6995. https://doi.org/10.1016/j.ijhydene.2021.03.180

Badea, Lestari, A.,Kurniasih, Y., Indah, D.R., and

Ahmadi. 2022. "Pengaruh variasi jumlah elektroda dan jenis katalis terhadap produksi gas hidrogen pada elektrolisis air laut." *JPIn 5(2)*, 562-572.

Chi, J., & Yu, H., 2018. "Water electrolysis based on renewable energy for hydrogen production." *Chin. J. Catal. 39(3)*, 390–394. https://doi.org/10.1016/S1872-2067(17)62949-8

Cho, H. H., Strezov, V., Evans, T. J., 2022. "Environmental impact assessment of hydrogen production via steam methane reforming based on emissions data." *Energy Rep*. 8, 13585-13595. https://doi.org/10.1016/j.egyr.2022.10.053

Finke, C.E., Leandri, H.F., Karumb, E.T., Zheng, D., Hoffmann, M.R., Fromer, N.A., 2021. "Economically advantageous pathways for reducing greenhouse gas emissions from industrial hydrogen under common, current economic conditions." *Energy Environ. Sci. 14(3)*, 1517–1529. https://doi.org/10.1039/D0EE03768K

Gielen, D., Taibi, E., dan Miranda, R., 2019. A Renewable Energy Perspective. 2nd Ed. International Renewable Energy Agency. Abu Dhabi.

Herlambang, Y. D., Kurnianingsih, Anis R., and Fatahul A., 2020. "Model Experimental of Photovoltaic-Electrolyzer Fuel Cells as a Small-Scale Power." *J. Phys.: Conf. Ser. 1700 012100*. https://doi.org/10.1088/1742-6596/1700/1/012100

House, J. E., & House, K. A. 2016. Hydrogen. In Descriptive Inorganic Chemistry, 3rd ed. Elsevier. pp. 111–121.

Huang X, Xu X, Luan X, and Cheng D., 2020. "CoP nanowires coupled with CoMoP nanosheets as a highly efficient cooperative catalyst for hydrogen evolution reaction." *Nano. Energy 68*, 104332. https://doi.org/10.1016/j.nanoen.2019.104332

Kim, Y. dan Lee, W. 2022. Seawater and Its Resources. Seawater Batteries. Green Energy and Technology. Springer, Singapore. 1-35.

Nairan A, Zou P, Liang C, Liu J, Wu D, Liu P, Yang C., 2019. "NiMo solid solution nanowire array electrodes for highly efficient hydrogen evolution reaction." *Adv. Funct. Mater. 29*, 1903747. https://doi.org/10.1002/adfm.201903747

Nascimento, S. F., Antônio J. N. D., Guilherme MM. S., Hugo S. D., Luís H. L. L., Wilma A. G., 2023. "Characterization of niobia-alumina deposited by the sol-gel process on carbon steel." *Mater. Res. 21(3)*, e20170525. http://dx.doi.org/10.1590/1980-5373-MR-2017-0525

Nikolaidis, P. dan Poullikkas, A., 2017. "A comparative overview of hydrogen production processes." *Renew. Sustain. Energy Rev. 67*, 597-611. https://doi.org/10.1016/j.rser.2016.09.044

Oraby, M. dan Shawqi A., 2024. "Green hydrogen production directly from seawater with no corrosion using a nonmetallic electrode: A novel solution and a proof of concept." *Int. J. Energy Res. 2*, 1-11. https://doi.org/10.1155/2024/5576626

Prastuti, O., 2017. "Pengaruh komposisi air laut dan pasir laut sebagai sumber energi listrik." *J. Tek. Kim. Lingk. 1*, 35-41.

Rahwanda, R., Putra, Y. S., dan Adriat, R., 2022. "Pemetaan dan estimasi potensi energi matahari di kota pontianak." *Prisma*

Fisika 10(3), 285 - 290.

Sangian, M. C., Mangindaan, G. M. C., dan Sangian, H. F., 2023. "Produksi hidrogen menggunakan teknik elektrolisis air dengan variabel kuat arus." *JTEK*. *12(1)*, 61-66.

Saputra, J., Toifur, M., Ishafit, dan Okimustaf., 2020. Pengaruh Waktu Deposisi pada Electroplating Cu/Ni Berbantuan Medan Magnet Sejajar. Universitas Ahmad Dahlan, Indonesia

Siddiqui, O., Dincer, I., 2019. "A well to pump life cycle environmental impact assessment of some hydrogen production routes." *Int. J. Hydrogen Energy 44*, 5773–5786. https://doi.org/10.1016/j.ijhydene.2019.01.118

Srour, T., Kumar, K., Martin, V., Dubau, L., Mailard, F., Gilles, B., Dillet, J., Didierjean, S., Amoury, B., dan Le, T.D., 2024. "On the contact resistance between the anode and the porous transport layer in a proton exchange membrane water electrolyzer." *Int. J. Hydrogen Energy 58,* 351-361. https://doi.org/10.1016/j.ijhydene.2024.01.134

Suliman MH, Adam A, Siddiqui MN, Yamani ZH, Qamar M., 2019. "Facile synthesis of ultrathin interconnected carbon nanosheets as a robust support for small and uniformly dispersed iron phosphide for the hydrogen evolution reaction." *Carbon 144*, 764-71. https://doi.org/10.1016/j.carbon.2018.12.106

Yang, H., Hu, Y., Huang, D., Xiong, T., Li, M., Balogun, M-S., and Tong, Y., 2019. "Efficient hydrogen and oxygen evolution electrocatalysis by cobalt and phosphorus dual-doped vanadium nitridenanowires." *Mater. Today Chem. 11*, 1-7. https://doi.org/10.1016/j.mtchem.2018.10.004

Yowanda, V.T., dan Lestari, A. D., 2021. "Studi potensi garam di utara khatulistiwa Kalimantan Barat." *JeLAST 8(2)*, 1-7.

Zhang, D. dan Ashraf, M. A., 2020. "Electrochemical fabrication of Ni–Mo nanostars with Pt-like catalytic activity for both electrochemical hydrogen and oxygen evolution reactions." *Int. J. Hydrogen Energy, 45(55)*, 30533-30546. https://doi.org/10.1016/j.ijhydene.2020.08.093